Electronic structure and surface properties of MgB_{2}(0001) upon oxygen adsorption

Chang-Eun Kim, Keith G. Ray, David F. Bahr, and Vincenzo Lordi

Phys. Rev. B **97**, 195416 — Published 10 May 2018

DOI: 10.1103/PhysRevB.97.195416

Electronic structure and surface properties of $MgB_2(0001)$ upon oxygen adsorption

Chang-Eun Kim,[1,2] Keith G. Ray,[2] David F. Bahr,[1] and Vincenzo Lordi[2,*]

[1] *School of Materials Engineering, Purdue University, West Lafayette, IN 47906-2045, USA*
[2] *Lawrence Livermore National Laboratory 7000 East Avenue, Livermore, CA 94550, USA*

We use density-functional theory to investigate the bulk and surface properties of MgB_2. The unique bonding structure of MgB_2 is investigated by Bader's atoms-in-molecules, charge density difference, and occupancy projected band structure analyses. Oxygen adsorption on the charge-depleted surfaces of MgB_2 is studied by a surface potential energy mapping method, reporting a complete map including low-symmetry binding sites. The B-terminated $MgB_2(0001)$ demonstrates reconstruction of the graphene-like B layer and the reconstructed geometry exposes a three-fold site of the sub-surface Mg, making it accessible from the surface. Detailed reconstruction mechanisms are studied by simulated annealing method based on *ab-initio* molecular dynamics and nudged elastic band calculations. The surface clustering of B atoms significantly modifies the B $2p$ states to occupy low energy valence states. The present work emphasizes that a thorough understanding of the surface phase may explain an apparent inconsistency in the experimental surface characterization of MgB_2. Furthermore, these results suggest that the surface passivation can be an important technical challenge when it comes to development of a superconducting device using MgB_2.

INTRODUCTION

MgB_2 is an interesting superconductor with high T_c,[1,2] in which a two-gap superconductivity originates from its anisotropic bonding structure. MgB_2 has an AlB_2 type crystal structure, where close packed Mg layers and graphene-like B layers alternate along the c axis of the hexagonal unit cell. MgB_2 shows a complex bonding structure consisting of ionic inter-layer bonding and covalent/metallic mixed in-plane bonding. The B and Mg are stabilized in the layered structure by ionic charge transfer: B in MgB_2 exhibits a graphene-like hexagonal layer, while bulk B is stable in a rhombohedral phase;[3] also, the Mg–Mg distance within the Mg layer of MgB_2 is considerably smaller than that of bulk Mg. Mg transfers most of its valence electrons to B layers, filling B $2p_z$ orbitals while reducing the Mg–Mg bonding distances due to the emptying of the outer shell. The surface of this binary compound can exhibit unique properties and structures, since this fundamental interlayer charge transfer mechanism that stabilizes the layers in bulk MgB_2 does not persist at the surface.

MgB_2 has displayed a uniquely disordered superconducting vortex structure.[4] To fully understand the observed disorder, it is important to address any potential surface phases in order to credibly attribute the observation to a bulk property of MgB_2. MgB_2 is also known for difficulties in obtaining consistent surface-sensitive spectra from scanning tunneling spectroscopy and Auger methods.[5–8] It is suggested that an unstable surface construction could be a reason for such measurement inconsistencies.[1,9,10] As bulk properties are further studied, it is equally important to work toward a better understanding of the surface, which often stands between the physical probe and the bulk domain of interest.[9]

A frequently observed impurity in MgB_2 is oxygen, and the surfaces and grain boundaries of MgB_2 are commonly under the influence of oxygen impurities in one form or another.[11,12] $MgB_2(0001)$ is a stable low-energy facet occurring in crystalline MgB_2 synthesis,[13] which experimentally exhibits trace oxygen despite vacuum conditions encountered during the pre-synthesis stage. To better understand the MgB_2 surface and further investigate any possible surface reconstructions, we consider B- and Mg-terminated MgB_2 surfaces in both the pristine case and under the influence of adsorbed oxygen. A stable low-energy surface orientation is more thermodynamically probable and experimentally relevant,[13] therefore, we focus on the $MgB_2(0001)$ surface as a first step. Interestingly, calculations show the Mg-terminated $MgB_2(0001)$ is more thermodynamically stable in terms of surface energy,[14] but experimental studies reported in several cases that boron-rich surface phase is observed in MgB_2, as well.[5,15,16] The present work explores a possible reconstruction pathway of the B-terminated surface triggered by surface-adsorbate interaction, causing formation of complex surface oxide phase.

We begin with the electronic structure of the bulk, explain how the unique layered structure is stabilized, and show that the electrophilic B-terminated surface suffers a spontaneous reconstruction under the influence of adsorbed oxygen. The calculated ionicity of bulk MgB_2 coincides with a previous study based on Phillips-van Vechten-Levine (PVL) dielectric theory,[17] where 96.8% ionicity of Mg–B bonding was reported. We compute the oxygen adsorption potential energy surface map for both Mg- and B-terminated surfaces of $MgB_2(0001)$ and further detail their electronic structures as well as oxygen diffusion transition state geometries. Simulated annealing based on *ab-initio* molecular dynamics (*ai*MD) is used to explore a possible reconstruction pathway in the vicinity of the adsorbed oxygen. Based on the simulated annealing, we develop a two-step reconstruction model of B-terminated $MgB_2(0001)$ with adsorbed oxygen and calculate the transition state energy barriers.

The results raise an interesting question of whether

the surface of MgB_2 retains its high T_c superconductivity. The high-T_c property of MgB_2 is known to originate from strong electron-phonon coupling, where in-plane $2p_{x,y}$ orbitals strongly couple to the in-plane E_{2g} phonon modes.[18,19] However, the present work shows that the E_{2g} mode does not exist in a reconstructed boron layer. Thus, the consequences of surface oxidation of MgB_2 can be more fundamental in destroying the superconductivity than mere dielectric formation.

METHODOLOGY

We perform density-functional theory calculations[20] using the Vienna *ab-initio* simulation package (VASP).[21,22] The kinetic energy cutoff for the planewave basis set is 500 eV and the electron-ion interactions are represented using the projector augmented wave (PAW) potentials.[23,24] The total energy convergence criterion is 10^{-5} eV for electronic minimization steps, and 10^{-4} eV for ionic displacement steps, which result in convergence of the Hellmann-Feynman forces to smaller than 10^{-4} eV/Å.

Various exchange-correlation functionals are tested, including LDA,[20] PBE,[25] PBEsol,[26] RPBE,[27] HSE06,[28–31] and PBE-D3.[32] We also used HSE(GW) method, where the HSE screening parameter is determined from quasiparticle GW calculation of the electronic structure of MgB_2.[33]

In regards to HSE(GW), the screened hybrid exchange-correlation functional allows two adjustable parameters to introduce and optimize the hybridization approach.[34] The two parameters α and μ respectively dictate the proportion of exact-exchange (Fock exchange calculated from DFT electron density) and the Coulombic screening parameter. The value α=0.25 is chosen such that the value, slope, and second derivative of the hybrid functional matches the semi-local functional in the non-interacting limit.[34] The μ parameter has been revised once,[28,30] and even suggested to be a material-specific parameter.[33] For MgB_2, the value μ=0.6 has been determined by fitting the electronic band structure and occupancies to quasiparticle GW calculations and resulted in significantly improved description of the structural, electronic, optical and vibronic properties.[33] There can be different ways to adjust the parameters in HSE functional, but we use α=0.25 and μ=0.6 in this study, and use a name HSE(GW) throughout the remaining text in order to underline the rationale of these so chosen parameters.

The theoretical lattice parameters of bulk MgB_2 are compared to experimental values.[35] The generalized-gradient approximation devised by Perdew, Burke and Ernzerhof (PBE)[25] is chosen for most of the calculations in this study, since it best reproduces the experimental structure and lattice constants. The choice of functional and comparison of theoretical and experimental structural parameters are discussed further in the Results and Discussion section. A Γ-centered 12×12×10 **k**-point grid is used for bulk structure relaxation, and 6×6×1 is used for surface and adsorption calculation for all the exchange-correlation functionals except HSE06 and HSE(GW). For HSE, we used a Γ-centered 6×6×3 for the bulk calculations, and 2×2×1 for $p(2\times2)$ supercell for the adsorption energy at high symmetry points. We use the HSE06 and HSE(GW) result to validate the PBE result, since the PBE functional is used in more computationally intensive calculations such as potential energy surface mapping, transition state calculations, and *ab initio* molecular dynamics. When not explicitly mentioned, the result is calculated using the PBE functional.

Occupancy-weighted, projected band structures are calculated in two steps. First, the ground state electronic density is calculated using a dense grid of 19×19×15 Γ-centered **k**-points. The band structures are then computed by keeping the charge density from the former step fixed and evaluating the eigenvalues on high-symmetry paths within the Brillouin zone.

The electronic charge density difference, $\Delta\rho$, is calculated by

$$\Delta\rho = \rho_{MgB_2} - \rho_{Mg} - \rho_{B}, \tag{1}$$

where ρ_{MgB_2} denotes the charge density of MgB_2 bulk, and ρ_{Mg} and ρ_{B} denote the charge density of Mg and B layers in the MgB_2 structure, respectively. The ρ_{Mg} and ρ_{B} terms are obtained by removing the other ions from the unit cell and calculating the corresponding ground state electronic charge densities. Visualization of Eq. (1) emphasizes the static charge transfer due to the interaction between Mg and B layers, where we use red and blue, respectively, to represent accumulation and depletion of electronic charge density.

The oxygen adsorption potential energy surface (PES) is obtained by computing the adsorption energy of O for a dense grid of points (about 20 points per Å^2) on the $MgB_2(0001)$ surface, allowing local relaxations, but constraining the in-plane coordinates of the O atom. A $p(2\times2)$ supercell is used (Fig. 1) for one adsorbed O atom, which corresponds to surface coverages θ = 0.125 ML for the B-terminated surface and θ = 0.25 ML for the Mg-terminated surface, while the areal density of oxygen is equal in both cases. Due to the hexagonal symmetry of the surfaces, only 1/12 of the area needs to be scanned in the actual calculation, enabling a dense sampling at an affordable computational cost.

The oxygen adsorption energy, E^{ad}, is calculated by

$$E^{ad} = E^{tot}_{O:MgB_2} - E^{tot}_{MgB_2} - n_O\mu_O, \tag{2}$$

where $E^{tot}_{O:MgB_2}$ denotes the total energy of oxygen adsorbed on $MgB_2(0001)$, $E^{tot}_{MgB_2}$ is the total energy of $MgB_2(0001)$, n_O is the number of adsorbed oxygen atoms, and μ_O denotes the chemical potential of oxygen. The parameter μ_O is a variable property of the oxygen that reflects the chemical environment. By using

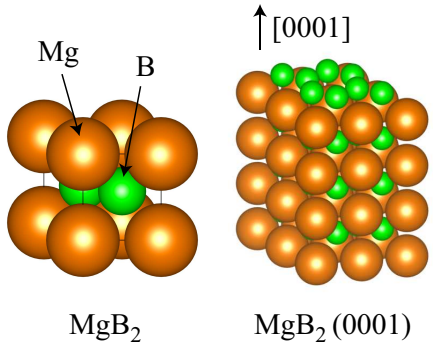

FIG. 1. (Color online) (left) Schematic representation of the MgB_2 bulk structure and (right) $MgB_2(0001)$ $p(2\times2)$ surface slab model. The vacuum distance in the $MgB_2(0001)$ slab model is about 16 Å.

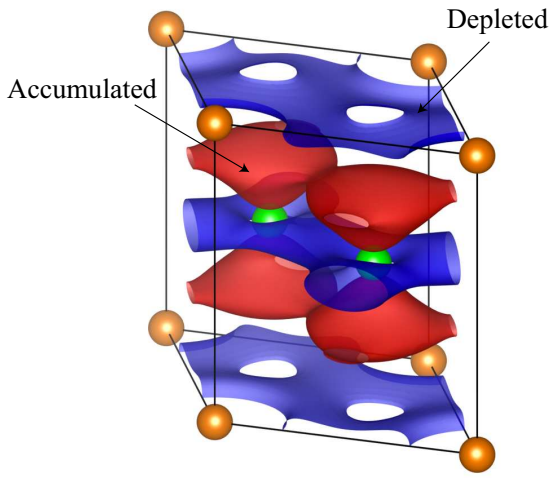

FIG. 2. (Color online) Electronic charge density difference plot of bulk MgB_2, as defined by Eq.1. An isosurface level of $0.034\,e/\text{Å}^3$ is shown. Electronic charge density accumulation is expressed in red color, the depletion is in blue color. The B $2p$ orbitals are filled with electrons transferred from Mg layer and also from in-plane σ bondings of B layer. Orange and green colored spheres represent Mg and B atoms, respectively.

the ground state total energy of an oxygen molecule, i.e., $\mu_O = 1/2E^{tot}_{O_2}$, we can obtain a first-principles prediction for the adsorption energy. However it is known that semi-local approximations suffer sizable self-interaction error, which can be improved by using hybrid functionals.[36] For this reason, the oxygen adsorption energy on the MgB_2 surface is calculated and compared with respect to different exchange-correlation functionals.

As will be discussed later, a severe reconstruction of the B-terminated surface is observed during the PES calculation. To further clarify the reconstruction mechanism, we investigate the oxygen-induced reconstruction of the B-terminated surface by using both *ab initio* molecular dynamics (*ai*MD)[38] simulations, as well as transition state calculations using the nudged elastic band (NEB) method. A $p(3\times3)$ supercell is used to explore a possible longer-range reconstruction pathway. The *ai*MD is performed in the canonical ensemble, based on the Nosé algorithm.[39] A time step of 1 fs, a kinetic energy cutoff of 400 eV, and a Γ-centered 2×2×1 **k**-point grid are used for the simulation, which was run for over 3 ps. The temperature control is set to 600 K with a Nosè period of 80 steps, providing sufficient thermal activation to capture the surface reconstruction within the limited duration.

We further explore the transition state energies using the nudged elastic band (NEB) method, where force-relaxed reconstructed snapshots are taken as the constraint configurations. Ten intermediate images are used for the transforming configurations between two constraints. A Γ-centered 4×4×1 **k**-point grid, kinetic energy cutoff of 400 eV, and dipole-corrections along the c axis are used with the $p(3\times3)$ supercell. A series of density-of-states calculations are performed for each transition state snapshot to examine the evolution of the electronic structure.

RESULTS AND DISCUSSION

The bulk lattice parameters of MgB_2, calculated using different exchange-correlation functionals, are listed in Table I. The generalized gradient approximation as formulated by Perdew, Burke, and Ernzerhof (PBE) is found to yield the closest agreement with experimental values. Although bulk MgB_2 has an alternating layered structure, the nature of the interlayer interaction is significantly different than van der Waals bonding.[40] While van der Waals layered materials typically exhibit strong covalent bonding in-plane and relatively weak interlayer coupling, in contrast, the interlayer interaction of MgB_2 is found to be ionic.[41] In fact, when we introduce weak-force corrections using the GGA-D3 scheme by Grimme,[32] the theoretical results deviate further from the experimental measurements, as seen in Table I.[35]

The ionic character of interlayer interaction of MgB_2 is evident from Bader's atoms-in-molecules charge analysis[43,44] of the charge transfer. In MgB_2, Mg transfers most of its valence charge ($\Delta\rho = -1.94e$/atom) to B ($\Delta\rho = +0.97e$/atom). The transferred charge leads to filling of B $2p_z$ orbitals as indicated by the plot of charge density difference, $\Delta\rho$, depicted in Fig. 2. In experiments, a refined x-ray diffraction study coupled with maximum entropy analysis[45] showed that the electron charge density is highly localized around the B layers.[46] The interesting electronic structure of this ionic layered material gives fundamental insight on how the anisotropic superconducting gap is established in MgB_2. In a graphene-like structure, elemental boron has insufficient valence electrons available to form π bonding states, since all 3

TABLE I. Lattice parameters of MgB_2 with respect to various exchange-correlation (xc) functionals. The percentage differences to the experimental measurement in Ref. 35 are shown in the parentheses.

xc	a	c
PBE	3.077 (−0.09)	3.509 (−0.02)
PBE-D3	3.054 (−0.86)	3.470 (−1.15)
PBEsol	3.067 (−0.41)	3.485 (−0.71)
RPBE	3.096 (+0.53)	3.544 (+0.98)
HSE06	3.055 (−0.81)	3.545 (+1.01)
HSE(GW)	3.060 (−0.65)	3.547 (+1.04)
LDA	3.036 (−1.43)	3.436 (−2.10)
Exp.(T=298 K)[35]	3.081	3.518
Exp.(T=37 K)[42]	3.082	3.515

valence electrons occupy in-plane σ bonds. However, in MgB_2, filling of the B $2p_z$ orbital by the valence charge transferred from Mg causes the boron layer to develop both σ bonding states and π bonding states, leading to the extraordinary two-gap superconducting gap states.[19]

It has been shown previously that the partially occupied σ bonding orbitals of the boron layer are strongly coupled with in-plane phonons.[19,47] The $\Delta\rho$ reported in this work shows further that the electron density of the boron σ bonds is slightly depleted as the interlayer charge transfer leads to formation of π bonding states (Fig. 2).

The occupancy resolved, projected electronic band structure of MgB_2 is shown in Fig. 3. Here the thickness of the lines conveys additional information of the occupancy and the colors indicate angular momentum of the Kohn-Sham eigenstates. Again, we find the B $2p$ states are filled, while Mg $3s$ state is empty in agreement with a previous DFT result using a different level of approximation.[48] This indicates ionic charge transfer from Mg $3s$ states to B $2p$, where the charge density difference result (Fig.2) suggests that the B $2p_z$ states are occupied. We also find the B $2s$ and B $2p$ states are smoothly mixed in the valence states, suggesting the presence of the sp^2 hybridization. The curvature of the band structure indicates both heavy ($\Gamma \rightarrow A$) and light ($H \rightarrow A$) effective masses of charge carriers at the Fermi level, which is suggestive of the complex Fermi surface.[19] In the MgB_2 unit cell, the path $\Gamma \rightarrow A$ corresponds to the momentum vector aligned with the layer-plane normal. The flat curvature of the eigenstates along that path indicates that the electron states are localized either on a Mg or B layer, further illustrating the ionic chemical interaction between the two elements. On the other hand, the highly-dispersive $H \rightarrow A$ path corresponds to an in-plane direction in the unit cell, revealing that the metallic in-plane bonding has free-electron-like character. The MgB_2 structure is sometimes described as an analogy of intercalated graphite.[46] Indeed, the addition of a Mg layer between B layers produces the unique electronic structure that resembles the sp^2 bonding network of graphene with a σ in-plane covalent bonding network and delocalized π bondings.

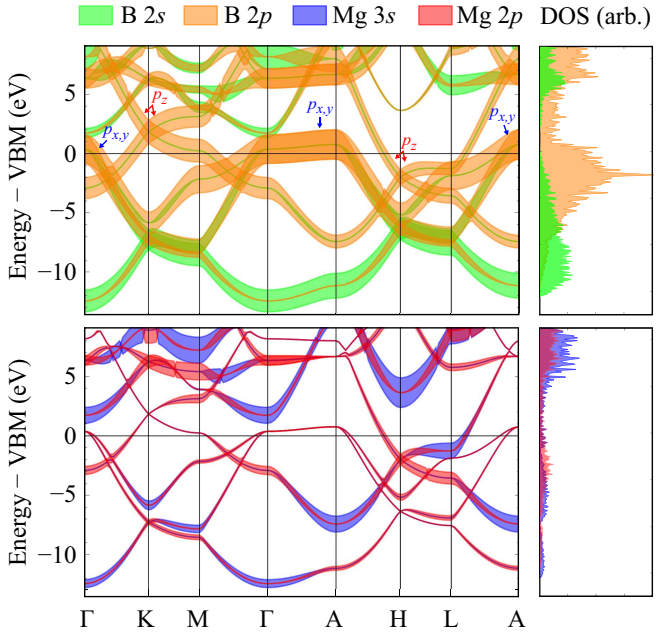

FIG. 3. (Color online) Projected electronic band structure of MgB_2 bulk. The thickness of each band indicates the occupancy weight of the eigenstates.

MgB_2 is a unique and interesting material in terms of the nature of its atomic bonding. The nearly complete charge transfer of valence electrons from Mg to B indicates ionic bonding character, as reflected by the Bader charge analysis, charge density differences, and band structure decompositions presented in this work, which is further consistent with previous PVL dielectric theory analysis.[17] However, the in-plane chemical interaction of the B layer is found to be covalent, while the out-of-plane interaction is mildly metallic.[49] These unique properties of bulk MgB_2 present important fundamental issues related to the surface properties of the material. Since the graphene-like structure of the B layer in MgB_2 is stabilized by charge transfer from the Mg layer, a question arises of whether the bare B-terminated $MgB_2(0001)$ surface exhibits an instability. Furthermore, the Mg layer in MgB_2 has significantly reduced interatomic distances compared to the pure Mg hexagonal closed packed (HCP) structure. Thus, detailed understanding of both B- and Mg-terminated $MgB_2(0001)$ surfaces is fundamentally important.

$MgB_2(0001)$ is a stable facet observed experimentally in synthesized MgB_2 single crystals.[13] In a previous experimental study, Auger spectroscopy of polycrystalline MgB_2 revealed both Mg-rich and B-rich phases of the MgB_2 surface.[5] Soft-x-ray spectroscopy of polycrystalline films showed evidence of surface boron oxides.[15] Yet another study on large-area deposited polycrystalline MgB_2 film reported both Mg and B oxides present on the

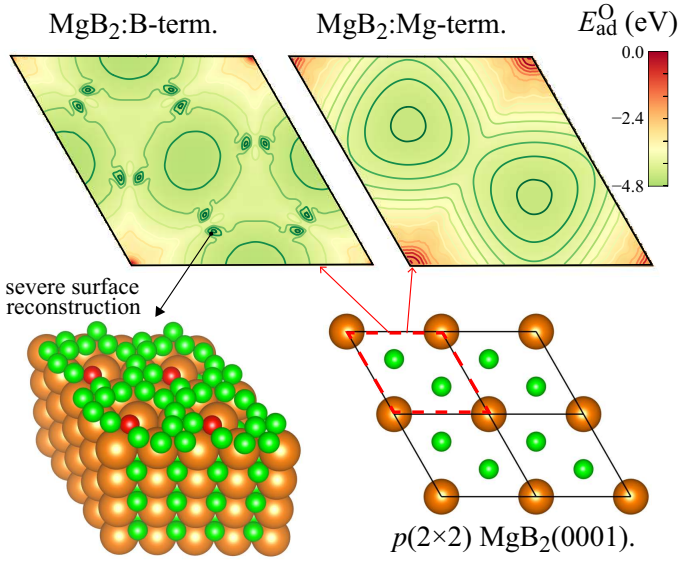

FIG. 4. (Color online) Calculated oxygen adsorption potential energy surface of $MgB_2(0001)$.

surface.[16] A series of oxidation tests on MgB_2 showed that annealing at 400 °C under oxygen flow resulted in formation of metastable surface oxide phase, substantially lowering the superconducting transition temperature of MgB_2.[50] These experimental observations offer useful insight and further motivate to investigate a probable metastable oxide phase of B-terminated surface, despite the Mg-terminated surface is found to have lower surface energy in its pristine phase.[14]

In our study, we use DFT to investigate the oxygen adsorption on both B- and Mg-terminated surfaces. We performed a full evaluation of the potential energy surface (PES) for oxygen adsorption across the entire unit cell of $MgB_2(0001)$, as opposed to evaluating the adsorption energy at only a few most-stable sites. The PES result is shown in Fig. 4. The oxygen adsorption on $MgB_2(0001)$ is in general exothermic, consistent with the experimental observation of oxygen surface contamination. The most stable oxygen adsorption sites are found to be the bridge sites of boron for the B-terminated surface and the three-fold sites of magnesium for the Mg-terminated surface. Note that the stability of B- or Mg-terminated surfaces is a function of the chemical potentials μ_B and μ_{Mg}. A previous DFT study suggested that Mg-terminated $MgB_2(0001)$ may be more stable than the B-terminated surface for a wide range of μ space, however, the result also shows that there exists a B-rich phase domain where B-terminated $MgB_2(0001)$ can be more stable.[41] The theoretical surface stability calculation assumes a homogeneous and ideal surface structure, and does not explain why mixed surface phases are found in experimental studies. Interestingly, later we show that a certain surface reconstruction of the B-terminated surface might be responsible for making the Mg sub-layer accessible from the surface, leading to both B- and Mg-mixed termination.

TABLE II. Oxygen adsorption energy, E_{ad}, in eV, computed using various exchange-correlation functionals for the different binding sites defined in Fig. 5 for both Mg- and B-terminated MgB_2. Here, we set $\mu_O = 1/2E^{tot}_{O_2}$. See the text for a description of the HSE(GW) functional.

Site	HSE06	HSE(GW)	LDA	PBED3	PBE	PBEsol	RPBE
A	-3.51	-4.30	-4.64	-4.29	-4.20	-4.25	-3.99
B	-0.56	-1.39	-1.77	-1.67	-1.56	-1.52	-1.44
C	-2.96	-3.70	-4.05	-3.75	-3.65	-3.69	-3.46
D	-2.80	-2.93	-2.85	-3.10	-2.66	-2.69	-2.54
E	-4.22	-3.34	-3.50	-3.36	-3.31	-3.29	-3.19
F	0.40	0.73	-0.24	0.09	0.21	-0.01	0.43
G	-4.76	-4.15	-4.54	-4.14	-4.08	-4.23	-3.85
H	-5.00	-4.42	-4.83	-4.40	-4.34	-4.50	-4.11

The DFT results of this study suggest two important phenomena: (i) both B- and Mg-terminated surfaces are prone to direct oxidation; and (ii) the B-terminated surface can exhibit severe reconstruction due to the absence of the Mg valence charge-transfer capping layer, as well as due to the intrinsic polymorphism of boron.[51,52] The Mg capping layer plays a crucial role in stabilizing the B-terminated surface. We find the Wigner-Seitz radii integration of electronic charge gives 1.925 e for B atoms covered under a Mg capping layer, however, this value decreases to 1.841 e for surface B atoms of the B-terminated surface, indicating that the presence of Mg capping layer plays a significant role in determining the charge state of B layers.

For the B-terminated surface, there exist a number of binding sites that initiate reconstruction of the surface boron structures. Boron is known to exhibit a number of energetically degenerate atomic arrangements.[51,52] The presence of such instabilities and complexity propose a possible reason why obtaining a consistent surface characterization of MgB_2 can be challenging.[6–8]

The precise reconstructed geometry reported in this study can be one of several various possible reconstruction modes, since the search for reconstructed geometry is constrained by the size and symmetry of the periodic supercell used; in fact, it is well known that pure B phases can exhibit very large primitive unit cells with more than 200 atoms.[54,55] For this reason, we may expect a wide variety of surface crystalline structure will be observed when the exposed Mg subsurface layer is oxidized and therefore chemical binding to the boron atoms on the top surface is weakened.

We use *ai*MD simulated annealing and the NEB method to identify and characterize the key reconstruction steps involved in oxygen adsorption at the surface. From the observed reconstruction reported in this study, we find generally that the surface boron atoms increase their coordination number substantially and deviate from

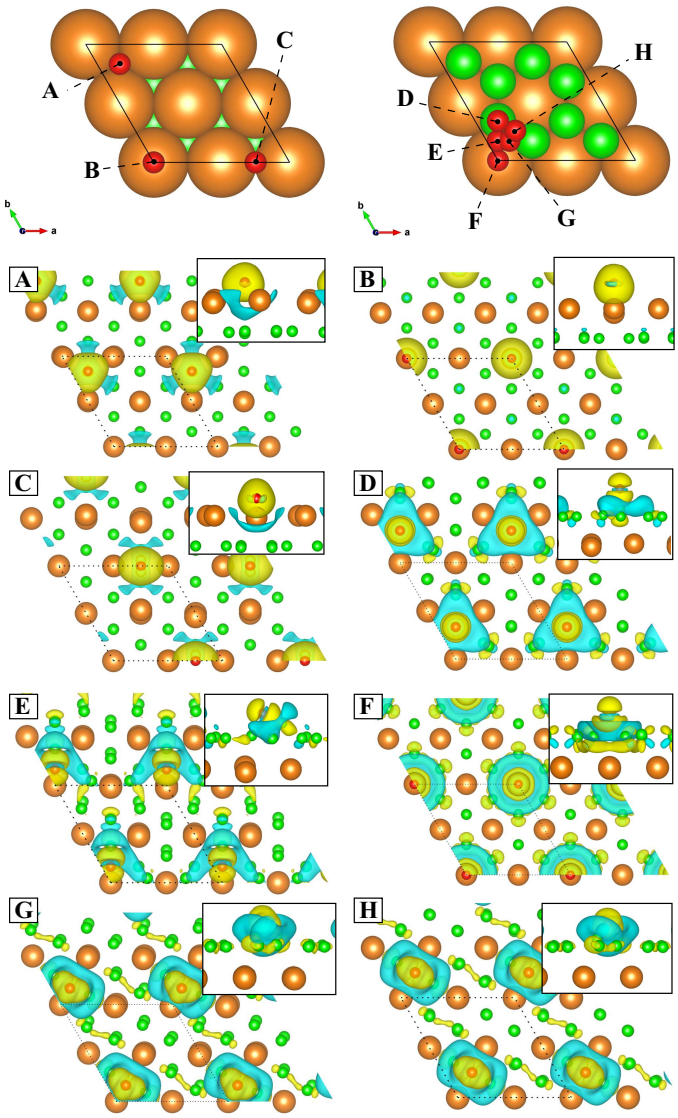

FIG. 5. (Color online) The high symmetry binding sites on Mg-terminated (upper-left) and B-terminated (upper-right) surfaces. The calculated oxygen adsorption energies with respect to various exchange-correlation functionals are listed in Table I. Corresponding charge density differences calculated at the PBE level for each binding site are shown in the lower plots. A constant isosurface level of 0.024 $e/\text{Å}^3$ is used to generate each of the volumetric representations of charge density. Top views are shown along with side views in the insets. Visualization software VESTA was used to create the images.[53] Yellow color represents electronic charge accumulation, cyan color represents depletion. For discussions in the text, we name the chosen binding sites as following: **A** Mg 3-fold, **B** Mg top, **C** Mg bridge, **D** B top, **E** B-Mg, **F** B 6-fold, **G** 2B-Mg, and **H** B bridge sites.

the honeycomb graphene-like geometry upon oxygen adsorption. On the other hand, no significant reconstruction is found in Mg-terminated $MgB_2(0001)$ for the oxygen coverage considered in this study ($\theta = 0.25$). The Mg atoms in the Mg-terminated surface have a significantly reduced Mg–Mg bonding distance (3.08 Å) compared to pure Mg, therefore the close-packed Mg layer in MgB_2 is stabilized by the B layer, which depletes the outer-shell electrons of Mg and reduces the effective radii of the ionized Mg atoms.

The calculated oxygen adsorption energies of high symmetry binding sites on B- and Mg-terminated $MgB_2(0001)$ are listed in Table II. The atomistic representation of the high symmetry binding sites are shown in Fig. 5, along with corresponding charge density difference plots. Overall, the oxygen adsorption is most favorable at Mg three-fold centers and B bridge sites. Comparison between HSE06 and HSE(GW) result is interesting because it demonstrates how the screening parameter, μ, can significantly influence the oxygen binding energy prediction. Note that the difference in the oxygen binding energy between the two functional is only 0.06 eV, which means the correction made by improving the screening parameter comes from the total energy of MgB_2 substrate. This observation underlines the significance of using optimized parameters for the hybrid functional. The binding energy calculated by HSE(GW) agrees well with other semi-local approximation, except for the B six-fold site that is not a stable adsorption site. We further observe that the PBE results are in close agreement with HSE(GW), further validating the use of PBE to describe structure, energetics, and charge transfer effects in MgB_2.

The spatial distribution of charge transfer between the substrate and oxygen is captured by charge density difference analysis on the PBE level (Fig. 5). The result reveals interesting surface-adsorbate interaction. For the Mg-terminated surface, the surface electronic density changes only in the vicinity of the adsorbed oxygen, involving only a few surface Mg atoms in direct contact with the oxygen. On the contrary, for the B-terminated case, the valence charge density is disrupted by the adsorbed oxygen atom beyond the range of the first neighbors, demonstrating that the oxidation of the B-terminated surface weakens the honeycomb structure of the surface B layer by disrupting the partially filled σ bonds (see **H** of Fig. 5), providing reasons to understand the oxygen induced reconstruction of the B terminated surface.

The representative snapshots of the surface reconstruction modes described by *aiMD* are shown in Fig. 6. The depicted disruption of the graphene-like B layer is found at a specific adsorption site from the PES result shown above in Fig. 4. The particular adsorption site is in the vicinity of the B bridge site, but with slightly off-centered coordination. To identify the details of the reconstruction process, we performed simulated annealing as well as NEB calculations. It turns out, it is not the specific site that produces the reconstruction, but rather the distortion of B–O–B angle that allows the local adsorbate–substrate pairs to overcome the shallow transition state energy. We found that oxygen adsorbed on the stable bridge site can also lead to surface reconstruction when a sufficient thermal energy is provided, demonstrated by the simulated annealing result. To identify the primary

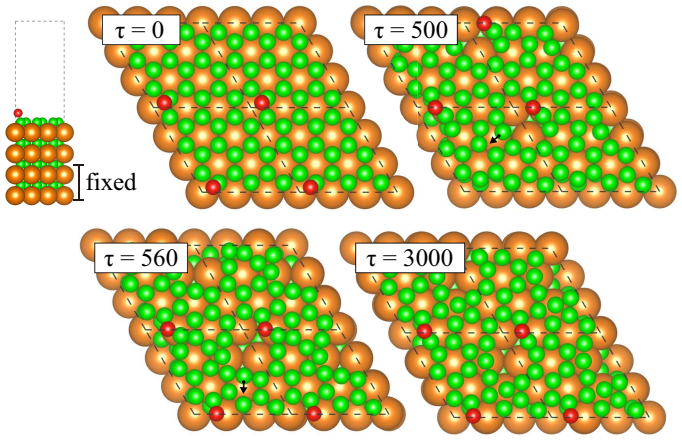

FIG. 6. (Color online) Simulated annealing representative snapshots with respect to the timesteps preceded. The control temperature, T=600 K, is used for this simulation to enhance kinetics. Oxygen adsorption at the B bridge site and reconstruction of the graphene-like B layers are clearly shown. The final configuration remained stable and did not fall back to the original configuration over the course of the simulation.

steps of the reconstruction, we use a $p(3\times3)$ B-terminated $MgB_2(0001)$ slab supercell to explore the thermally activated trajectory of the surface borons. The trajectory calculated at T=600 K reveals a key transition process of the reconstruction, from which we determine a series of static configurations and perform NEB calculations to estimate the transition state energies.

Based on the *ai*MD trajectories, we construct model structures that represent the key stages of reconstruction, followed by high-precision geometric optimizations. Once the ground state geometry is obtained, we perform NEB calculations to estimate the transition energy barrier of each boron migration process. The NEB results, obtained by using force-relaxed geometries of the static configurations, are shown in Fig. 7. The activation energy is found to be the range of 0.1-0.2 eV. The thermodynamic driving force behind the migration process mainly originates from the changes in electronic structure of B $2p$ states. A series of density-of-state (DOS) calculations are performed for each configuration along the transition pathways (see Fig. 7). These results show a decrease in the DOS corresponding to σ bonding in the B plane, *i.e.*, B $2p$ states with energies near and just below the Fermi level, for nearly all boron atoms involved in both migration pathways, (a) to (b) and (b) to (c). Notably, the DOS for the Mg $3s$ states increases during the migration, showing that the increased coordination of the B atoms is associated with a smaller charge transfer from the Mg atoms.

The NEB result indicates that the surface migration of B is a downhill process with an exothermic energy difference of −0.8 eV. The NEB results are consistent with the *aiMD* results presented above, where thermal activation was needed to trigger the reconstruction and the

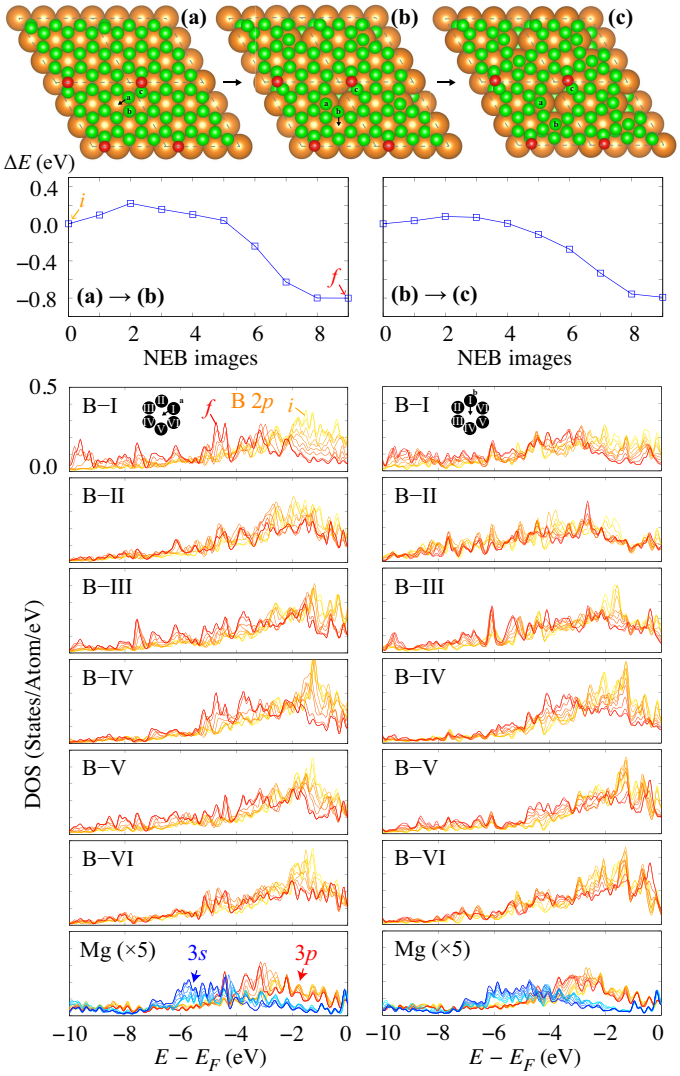

FIG. 7. (Color online) Nudged elastic band (NEB) result showing the energy and electronic structures associated with the key transition stages of the oxygen-induced reconstruction of B-terminated $MgB_2(0001)$.

reconstructed geometry remained stable. In a more general context, the reconstruction also can be triggered by other impurities that weaken the B–B partially filled σ bonds, since the migration of surface B atoms is a rapid downhill process. The HSE(GW) calculations for the reconstruction model qualitatively agree with the PBE result, showing −1.0 eV and −0.5 eV energy differences for the transition from (a) to (b) and (b) to (c), respectively.

The theoretical results in the present work suggest that the consequences of oxidation of MgB_2 are not limited to a simple formation of a dielectric layer. Instead, a significant reconstruction of the surface termination layer can occur even at relatively low O adsorbate coverages. The reconstruction disrupts the graphene-like structure of the B layer, rendering the key process that enables high T_c superconductivity in MgB_2—namely, E_{2g} phonon mode

coupling to the in-plane electronic states—no longer available. A potential consequence of having a spontaneous reconstruction pathway in this binary layer compound is that the disrupted phase may not be localized to the surface, making the surface disordering more substantial. The relatively small-scale simulation reported in this work already shows that such a reconstruction of B-terminated layer can expose the three-fold site of Mg sub-layer, as shown in Fig. 7, and further complexity is likely over longer distance scales of the surface. It is important to investigate further how this subtle phase disordering can influence surface-sensitive characterization experiments, such as scanning tunneling spectroscopy[6–8] or magnetic spectroscopy of the vortex structure.[4] Previous experimental study on nanoscale MgB_2 thin film (reported thickness of about 400 nm) showed that removal of surface layer of $MgB_2(0001)$ by chemical etching led to increase of the superconductivity gap energy by 25 % as measured by scanning tunneling spectroscopy.[56] A series of ultrathin film study showed the transition temperature (T_c) decreases with respect to increasing surface-to-bulk ratio of the thin MgB_2 films,[57] in agreement with the suggested idea in the present work. A surface modification strategy may be necessary in order to improve surface stability of MgB_2 thin films.[58]

Much effort has been focused on understanding the relation between the surface states and the superconductivity of thin film MgB_2.[58–61] A hypothesis has been presented that ultrathin film MgB_2 can have different T_c than bulk material, due to interaction between the surface electronic structure and the surface phonons of MgB_2 ultrathin film. Those theoretical results are mainly based on non-reconstructed pristine $MgB_2(0001)$ surfaces. The present work suggests a new possibility where surface reconstruction can play an important role in the thin film superconductivity of MgB_2. For example, a prior theoretical work showed the B-terminated surface can introduce significantly increased electronic density of states (DOS) at the Fermi level, $N(E_F)$.[60] The increase of $N(E_F)$ could be interpreted as to potentially enhance the surface superconductivity within the view of the quasielastic approximation. However, the present work shows that $N(E_F)$ can actually decrease by reconstruction of the B-terminated MgB_2 surface (Fig. 7). The electron-phonon coupling of the surface states and the surface phonons might deviate from the pristine case due to the absence of E_{2g} modes in the reconstructed surface, as well. We hope the present work provides useful clues to understand the role of oxygen adsorption on introducing any discrepancies in the experimental measurements compared to the theoretical prediction based on pristine MgB_2 surface models.

CONCLUSIONS

The surface stability of $MgB_2(0001)$ under the influence of adsorbed oxygen is investigated by density-functional theory calculations. The B-terminated $MgB_2(0001)$ surface is found to undergo significant reconstruction in the present of even small amounts of oxygen. An oxygen adsorbed at the B bridge site can weaken the surface B–B σ bondings, leading to a series of B migrations that result in lowering the total energy by 0.8 eV. Low transition state energies in the range of 0.1-0.2 eV are found for this process. The opening of B-terminated layer during reconstruction results in the exposure of a three-fold site of the sub-surface Mg. The present work identifies a reconstruction mechanism of B-terminated MgB_2 that makes its subsurface layer more prone to contaminates and potential reconstruction once chemical and thermal perturbations are introduced. The present work also suggests a proper interpretation of any surface-sensitive characterization experiment may require a rigorous surface structural/chemical characterization in order to guarantee the consistency of the measurement. In addition, we conclude that surface passivation can be an important technical challenge for successful development of high T_c superconducting devices made from MgB_2.

ACKNOWLEDGEMENT

This work was performed under the auspices of the U.S. Department of Energy by Lawrence Livermore National Laboratory under Contract DE-AC52-07NA27344, funded by the Laboratory Directed Research and Development Program at LLNL under project tracking code 15-ERD-051.

* Corresponding author.
E-mail: lordi2@llnl.gov

[1] F. Bouquet, R. A. Fisher, N. E. Phillips, D. G. Hinks, and J. D. Jorgensen, Phys. Rev. Lett. **87**, 047001 (2001).
[2] Y. Wang, T. Plackowski, and A. Junod, Physica C Supercond. **355**, 179 (2001).
[3] B. F. Decker and J. S. Kasper, Acta Crystallogr. **12**, 503 (1959).
[4] V. Moshchalkov, M. Menghini, T. Nishio, Q. H. Chen, A. V. Silhanek, V. H. Dao, L. F. Chibotaru, N. D. Zhigadlo, and J. Karpinski, Phys. Rev. Lett. **102**, 117001 (2009).
[5] M. Xu, Y. Takano, T. Hatano, T. Kimura, and D. Fujita, Appl. Surf. Sci. **205**, 225 (2003).
[6] G. Karapetrov, M. Iavarone, W. K. Kwok, G. W. Crabtree, and D. G. Hinks, Phys. Rev. Lett. **86**, 4374 (2001).
[7] G. Rubio-Bollinger, H. Suderow, and S. Vieira, Phys. Rev. Lett. **86**, 5582 (2001).
[8] P. Seneor, C. T. Chen, N. C. Yeh, R. P. Vasquez, L. D. Bell, C. U. Jung, M.-S. Park, H.-J. Kim, W. N. Kang, and

S.-I. Lee, Phys. Rev. B **65**, 012505 (2001).
[9] H. Schmidt, J. F. Zasadzinski, K. E. Gray, and D. G. Hinks, Phys. Rev. B **63**, 220504 (2001).
[10] A. Sharoni, I. Felner, and O. Millo, Phys. Rev. B **63**, 220508 (2001).
[11] R. K. Singh, Y. Shen, R. Gandikota, J. M. Rowell, and N. Newman, Supercond. Sci. Technol. **21**, 015018 (2007).
[12] R. F. Klie, J. C. Idrobo, N. D. Browning, K. A. Regan, N. S. Rogado, and R. J. Cava, Appl. Phys. Lett. **79**, 1837 (2001).
[13] W. Chen, W. Liu, C. Chen, R. Wang, and Q. Feng, CrystEngComm **13**, 3959 (2011).
[14] Y. Wang, K. Michel, Y. Zhang, and C. Wolverton, Phys. Rev. B **91**, 155431 (2015).
[15] T. A. Callcott, L. Lin, G. T. Woods, G. P. Zhang, J. R. Thompson, M. Paranthaman, and D. L. Ederer, Phys. Rev. B **64**, 132504 (2001).
[16] B. H. Moeckly and W. S. Ruby, Supercond. Sci. Technol. **19**, L21 (2006).
[17] X. L. Chen, Q. Y. Tu, M. He, L. Dai, and L. Wu, J. Phys.: Condens. Matter **13**, L723 (2001).
[18] A. Y. Liu, I. I. Mazin, and J. Kortus, Phys. Rev. Lett. **87**, 087005 (2001).
[19] H. J. Choi, D. Roundy, H. Sun, M. L. Cohen, and S. G. Louie, Nature **418**, 758 (2002).
[20] W. Kohn and L. J. Sham, Phys. Rev. **140**, A1133 (1965).
[21] G. Kresse and J. Furthmuller, Phys. Rev. B **54**, 11169 (1996).
[22] G. Kresse and J. Furthmuller, Comp. Mater. Sci. **6**, 15 (1996).
[23] P. E. Blöchl, Phys. Rev. B **50**, 17953 (1994).
[24] G. Kresse and D. Joubert, Phys. Rev. B **59**, 1758 (1999).
[25] J. P. Perdew, K. Burke, and M. Ernzerhof, Phys. Rev. Lett. **77**, 3865 (1996).
[26] J. P. Perdew, A. Ruzsinszky, G. I. Csonka, O. A. Vydrov, G. E. Scuseria, L. A. Constantin, X. Zhou, and K. Burke, Phys. Rev. Lett. **100**, 136406 (2008).
[27] B. Hammer, L. B. Hansen, and J. K. Nørskov, Phys. Rev. B **59**, 7413 (1999).
[28] J. Heyd, G. E. Scuseria, and M. Ernzerhof, J. Chem. Phys. **118**, 8207 (2003).
[29] J. Heyd and G. E. Scuseria, J. Chem. Phys. **121**, 1187 (2004).
[30] J. Heyd, G. E. Scuseria, and M. Ernzerhof, J. Chem. Phys. **124**, 219906 (2006).
[31] J. Paier, M. Marsman, K. Hummer, G. Kresse, I. C. Gerber, and J. G. ngyn, J. Chem. Phys. **124**, 154709 (2006).
[32] S. Grimme, J. Antony, S. Ehrlich, and H. Krieg, J. Chem. Phys. **132**, 154104 (2010).
[33] Z. P. Yin, A. Kutepov, and G. Kotliar, Phys. Rev. X **3**, 021011 (2013).
[34] J. P. Perdew, M. Ernzerhof, and K. Burke, J. Chem. Phys. **105**, 9982 (1996).
[35] H. Lun-hua, H. Gui-qing, Z. Pan-lin, and Y. Qi-wei, Chin. Phys. Soc. **10**, 343 (2001).
[36] S. Klüpfel, P. Klüpfel, and H. Jónsson, J. Chem. Phys. **137**, 124102 (2012).
[37] N. A. Richter, C.-E. Kim, C. Stampfl, and A. Soon, Phys. Chem. Chem. Phys. **16**, 26735 (2014).
[38] G. Kresse and J. Hafner, Phys. Rev. B **49**, 14251 (1994).
[39] S. Nosé, J. Chem. Phys. **81**, 511 (1984).
[40] A. K. Geim and I. V. Grigorieva, Nature **499**, 419 (2013).
[41] Z. Li, J. Yang, J. G. Hou, and Q. Zhu, Phys. Rev. B **65**, 100507 (2002).
[42] J. D. Jorgensen, D. G. Hinks, and S. Short, Phys. Rev. B **63**, 224522 (2001).
[43] W. Tang, E. Sanville, and G. Henkelman, J. Phys-Condens. Mat. **21**, 084204 (2009).
[44] R. F. W. Bader, *Atoms in Molecules* (Clarendon Press, 1990).
[45] D. M. Collins, Nature **298**, 49 (1982).
[46] E. Nishibori, M. Takata, M. Sakata, H. Tanaka, T. Muranaka, and J. Akimitsu, J. Phys. Soc. Jpn. **70**, 2252 (2001).
[47] J. M. An and W. E. Pickett, Phys. Rev. Lett. **86**, 4366 (2001).
[48] J. A. Silva-Guillén, Y. Noat, T. Cren, W. Sacks, E. Canadell, and P. Ordejón, Phys. Rev. B **92**, 064514 (2015).
[49] K. D. Belashchenko, M. van Schilfgaarde, and V. P. Antropov, Phys. Rev. B **64**, 092503 (2001).
[50] K. A. Yates, Z. Lockman, A. Kursumovic, G. Burnell, N. A. Stelmashenko, J. L. MacManus Driscoll, and M. G. Blamire, Appl. Phys. Lett. **86**, 022502 (2005).
[51] T. Ogitsu, F. Gygi, J. Reed, M. Udagawa, Y. Motome, E. Schwegler, and G. Galli, Phys. Rev. B **81**, 020102 (2010).
[52] T. Ogitsu, E. Schwegler, and G. Galli, Chem. Rev. **113**, 3425 (2013).
[53] K. Momma and F. Izumi, J. Appl. Crystallogr. **44**, 1272 (2011).
[54] T. Ogitsu, F. Gygi, J. Reed, Y. Motome, E. Schwegler, and G. Galli, J. Am. Chem. Soc. **131**, 1903 (2009).
[55] M. Widom and M. Mihalkovič, Phys. Rev. B **77**, 064113 (2008).
[56] F. Bobba, D. Roditchev, R. Lamy, E. M. Choi, H. J. Kim, W. N. Kang, V. Ferrando, C. Ferdeghini, F. Giubileo, and W. Sacks, Supercond. Sci. Technol. **16**, 167 (2002).
[57] Y. Zhang, Z. Lin, Q. Dai, D. Li, Y. Wang, Y. Zhang, Y. Wang, and Q. Feng, Supercond. Sci. Technol. **24**, 015013 (2010).
[58] V. Despoja, D. J. Mowbray, and V. M. Silkin, Phys. Rev. B **84**, 104514 (2011).
[59] V. M. Silkin, E. V. Chulkov, and P. M. Echenique, Phys. Rev. B **64**, 172512 (2001).
[60] G. Profeta, A. Continenza, F. Bernardini, and S. Massidda, Phys. Rev. B **66**, 184517 (2002).
[61] V. D. P. Servedio, S. L. Drechsler, and T. Mishonov, Phys. Rev. B **66**, 140502 (2002).